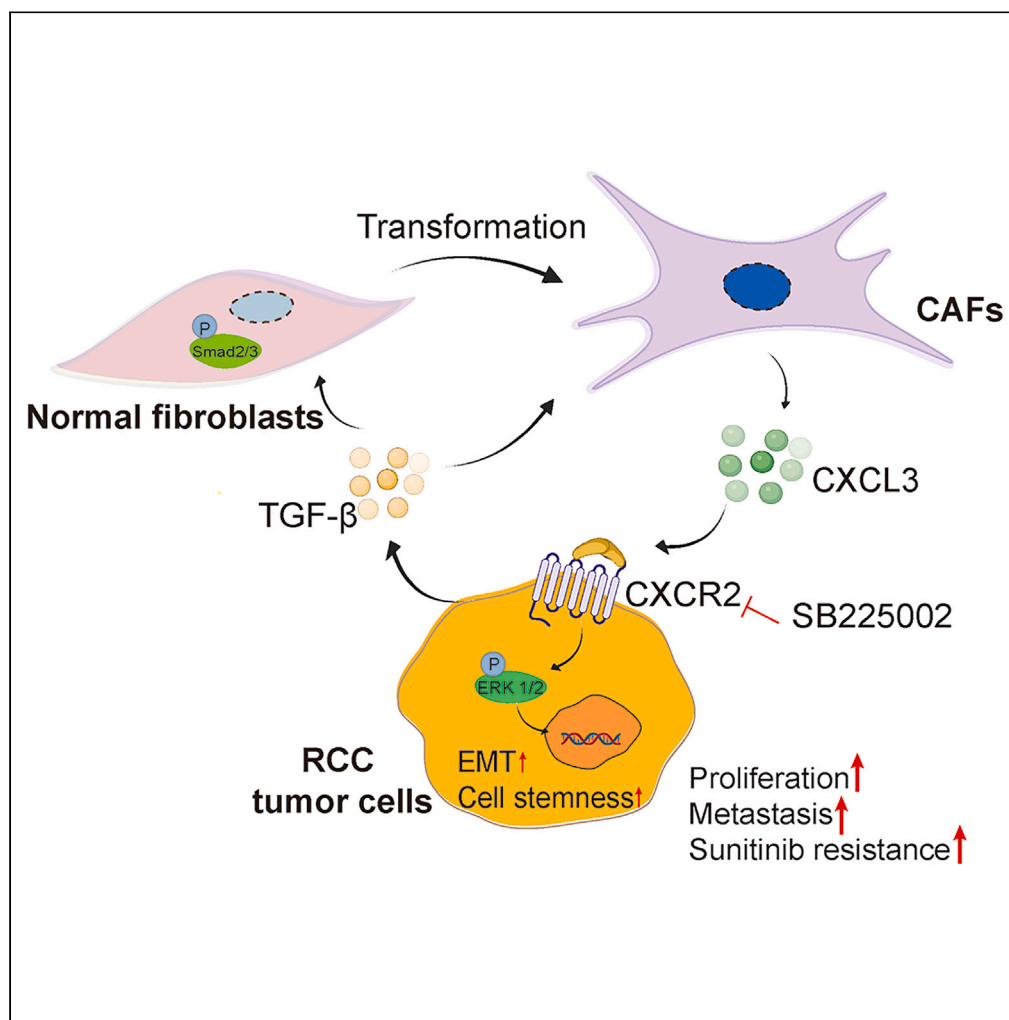# iScience

Article

CXCL3/TGF-β-mediated crosstalk between CAFs and tumor cells augments RCC progression and sunitinib resistance

Yunxia Wang,
Weihong Ding,
Wenjing Hao, ...,
Ke Xu, Weimin Cai,
Yuan Gao

weimincai@fudan.edu.cn (W.C.)
yuan_gao@fudan.edu.cn (Y.G.)

Highlights

CXCL3 derived from CAFs promoted RCC progression and sunitinib resistance

Tumor cells promoted the transformation of NFs and the expression of CXCL3

CXCR2 inhibitor SB225002 blocked the interaction between CAFs and tumor cells

iScience

Article

CXCL3/TGF-β-mediated crosstalk between CAFs and tumor cells augments RCC progression and sunitinib resistance

Yunxia Wang,[1,4] Weihong Ding,[2,4] Wenjing Hao,[1] Luyao Gong,[1] Yeheng Peng,[1] Jun Zhang,[1] Zhiyu Qian,[3] Ke Xu,[2] Weimin Cai,[1,*] and Yuan Gao[1,5,*]

SUMMARY

Cancer-associated fibroblasts (CAFs) play a significant role in tumor development and treatment failure, yet the precise mechanisms underlying their contribution to renal cell carcinoma (RCC) remains underexplored. This study explored the interaction between CAFs and tumor cells, and related mechanisms. CAFs isolated from tumor tissues promoted the tumor progression and drugs resistance both *in vivo* and *in vitro*. Mechanistically, chemokine (C-X-C motif) ligand (CXCL) 3 secreted from CAFs mediated its effects. CXCL3 activated its receptor CXCR2 to active the downstream ERK1/2 signaling pathway, subsequently promoting epithelial-mesenchymal transition and cell stemness. Blocking the crosstalk between CAFs and tumor cells by CXCR2 inhibitor SB225002 attenuated the functions of CAFs. Furthermore, Renca cells facilitated the transformation of normal interstitial fibroblasts (NFs) into CAFs and the expression of CXCL3 through TGF-β-Smad2/3 signaling pathway. In turn, transformed NFs promoted the tumor progression and drug resistance of RCC. These findings may constitute potential therapeutic strategies for RCC treatment.

INTRODUCTION

Renal cell carcinoma (RCC) is the most prevalent form of malignant renal parenchyma carcinoma, accounting for approximately 90% of renal malignancies and 3 to 5% of systemic malignancies.[1,2] The pathogenesis of RCC is notably complex, which complicates treatment efforts. Consequently, many patients with RCC experience poor outcomes and develop metastasis. This underscores the urgent need to delve deeper into the mechanisms behind, driving RCC development and to identify more effective therapeutic targets and strategies.

The tumor microenvironment (TME) plays a crucial role in tumor progression, consisting of tumor cells, immune and inflammatory cells, cancer-associated fibroblasts (CAFs), and complex network of interstitial tissue, cytokines, and chemokines.[3,4] As the most important stromal cells, CAFs have been shown to participate in the tumor occurrence and progression.[5] Usually, CAFs can secrete cytokines such as stromal cell derived factor 1, interleukin 6, and chemokine (C-X-C motif) ligand (CXCL), to augment tumor proliferation, metastasis, and drug resistance.[6–8] Nevertheless, the precise underlying mechanisms by which CAFs influence RCC progression remain poorly understood. Furthermore, CXCL3, a secretory growth factor involved in tumor cell migration, invasion and angiogenic regulation by activating CXC chemokine receptor (CXCR) 2. This molecule is highly expressed in pancreatic cancer,[9] prostate cancer,[10] breast cancer,[11] and colon cancer,[12] and is closely associated with their progression. The activation CXCR2 triggers the phosphorylation of downstream signal transduction pathways such as Raf-MEK-ERK, leading to tumor progression through downstream cascades.[13–15] CXCL3 and CXCR2 were significantly elevated in plasma and tumor tissues of patients with metastatic RCC.[16] However, to our knowledge, the specific mechanism of how CXCL3 regulates RCC metastasis and drug resistance has not been reported.

Tumor cells and immune cells can release a multitude of factors, including TGF-β1, osteopontin, and IL-1β to orchestrate the conversion of normal interstitial fibroblasts (NFs) into CAFs by modulating the TGF-β signaling pathways.[17,18] Tumor-derived exosomes can also transport TGF-β1 into fibroblasts, and subsequently reprogram NFs to CAFs through downstream mitogen-activated protein kinase (MAPK), NF-κB, transcription activator 3 (STAT3), or TGF-β signaling cascades, further amplifying the tumor progression.[19,20] Such transformations are critical, yet the detailed crosstalk between CAFs and tumor cells in RCC remains underexplored.

[1]School of Pharmacy, Fudan University, Shanghai 201203, China
[2]Department of Urology, Huashan Hospital, Fudan University, Shanghai 200040, China
[3]Department of Urology, Zhongshan Hospital, Fudan University, Shanghai 200032, China
[4]These authors contributed equally
[5]Lead contact
*Correspondence: weimincai@fudan.edu.cn (W.C.), yuan_gao@fudan.edu.cn (Y.G.)
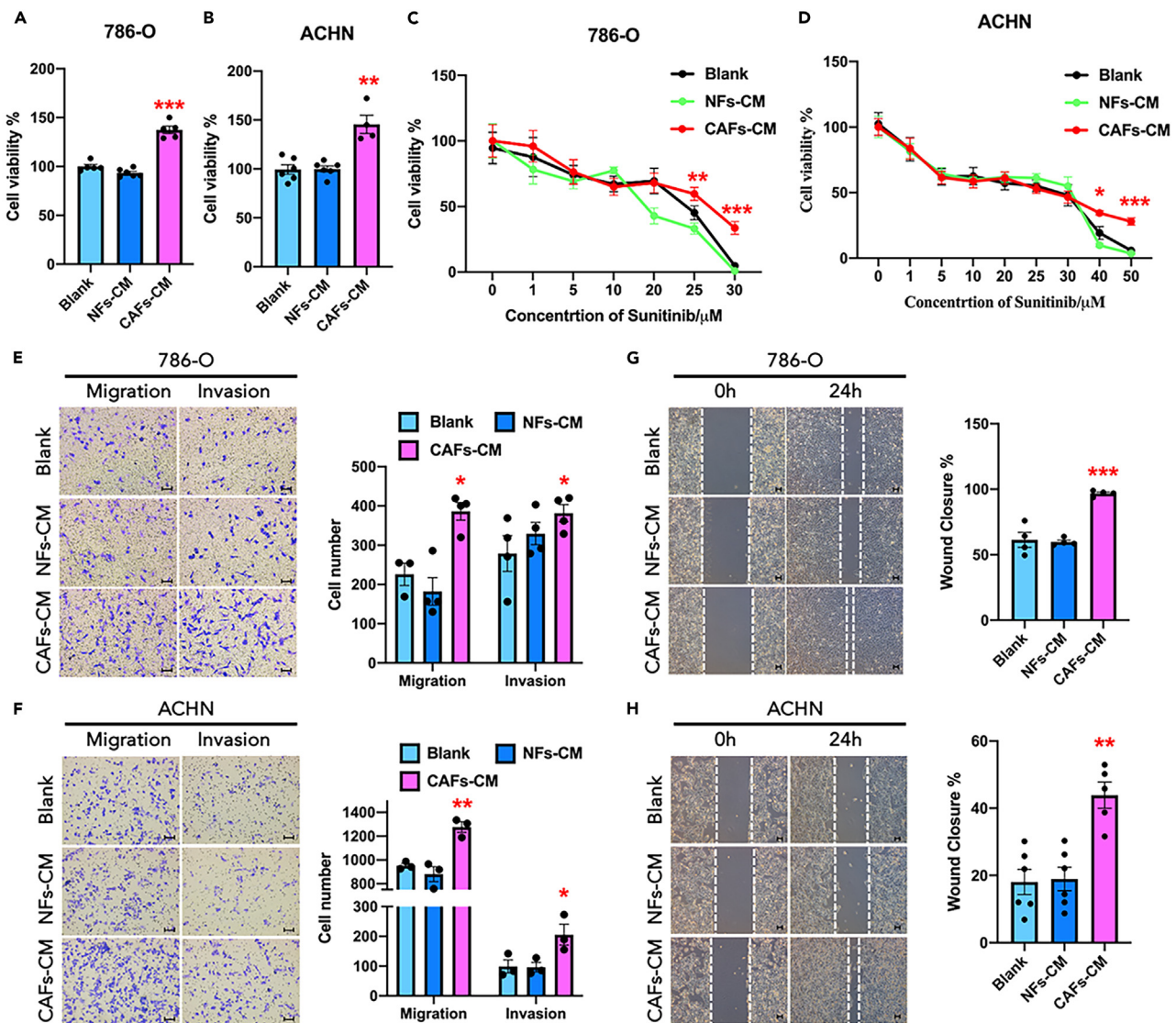https://doi.org/10.1016/j.isci.2024.110224

Figure 1. CAFs from RCC tissues enhanced proliferation, migration, and drug resistance of 786-O and ACHN cells

(A and B) Cell viability% of 786-O and ACHN cells cultured with CAFs-CM or NFs-CM.

(C and D) Cytotoxicity of sunitinib at different concentrations on 786-O and ACHN under the condition of CAFs-CM co-culture (to exclude the impact of cell proliferation, the absorbance value of sunitinib at a concentration of 0 μM was used as a control in the CAFs-CM group and NFs-CM group, respectively).

(E and F) Crystal violet staining and quantification of migrated and invasive 786-O and ACHN cells after 24 h treatment.

(G and H) Wound healing assay and quantification of 786-O and ACHN at 0 h and after 24 h treatment. NFs-CM represents a 1:1 mixture of tumor-adjacent normal fibroblast conditioned medium and fresh culture medium, while CAFs-CM represents a 1:1 mixture of human-derived CAFs conditioned medium and fresh culture medium. Scale bar: 100 μm. Data are shown as mean ± SEM, $n = 3 \sim 6$, $*p < 0.05$, $**p < 0.01$, $***p < 0.001$.

In present research, we observed increased CAFs infiltration in tumor tissues of RCC patients. The CAFs extracted from tumor tissues promoted RCC migration and proliferation, facilitating sunitinib resistance by CXCL3 paracrine. We also found that tumor cells promote the transition of NFs into CAFs and CXCL3 secretion through TGF-β-Smad2/3 signaling. Our findings offer a potential perspective on RCC treatment.

RESULTS

Patient-derived CAFs enhanced the proliferation, migration, and resistance to sunitinib of renal cancer cells

RNA sequencing (RNA-seq) data analysis indicated increased estimate score and stromal score in tumor tissues (Figures S1A–S1C), and the increased proportion of CAFs with the progression of tumor stage, as determined by estimating the proportion of immune and cancer cells (EPIC) analysis (Figures S1D–S1F). Furthermore, patients with higher expression of the CAFs signature genes (*COL5A1*, *COL16A1*, *EMILIN1*,
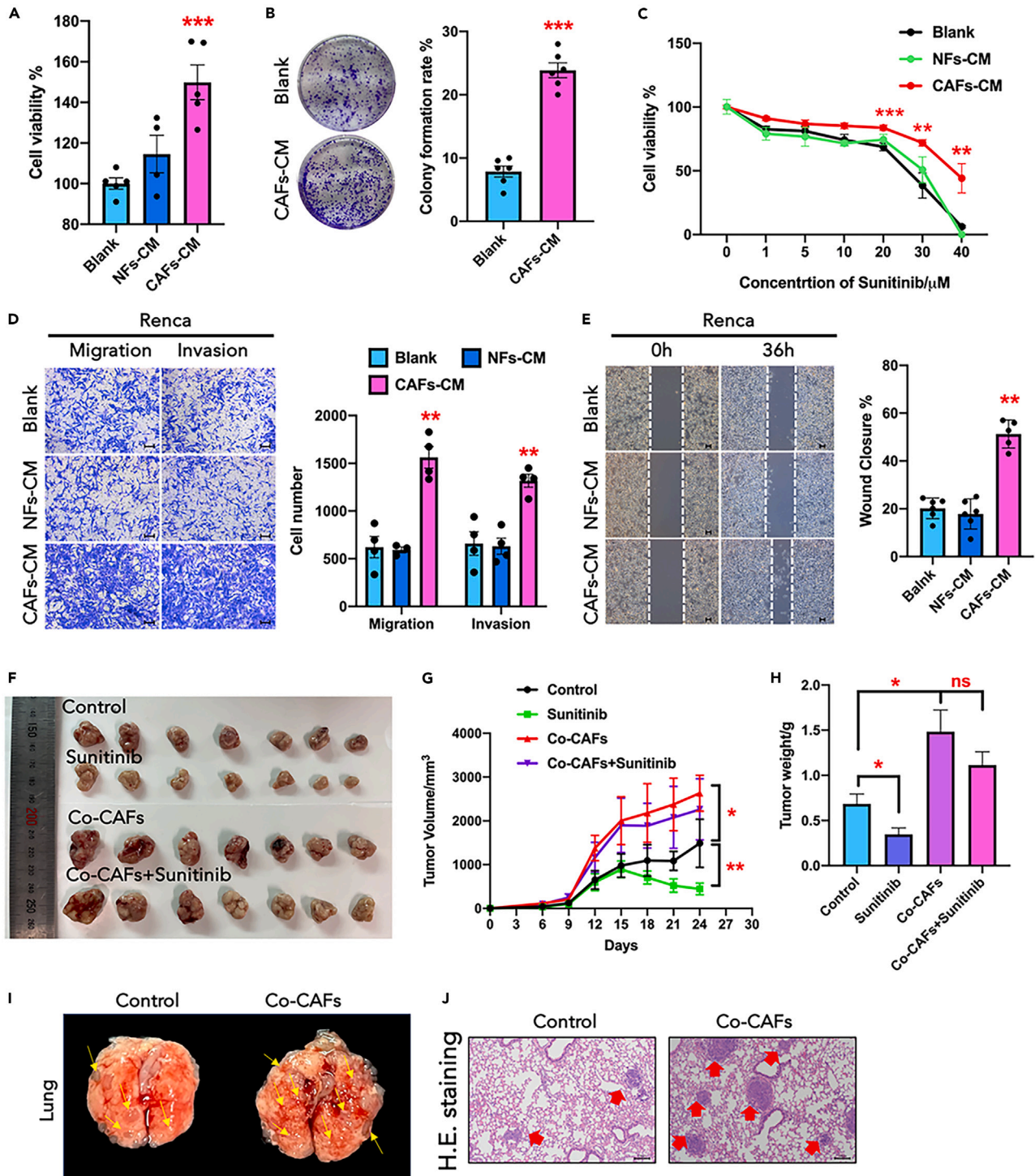
Figure 2. Mouse-derived CAFs promoted the progression and drug resistance of RCC

(A) Renca cells viability% co-cultured with CAFs-CM and NFs-CM.

(B) Crystal violet staining and quantification of colony formation.

(C) Sunitinib cytotoxicity at different concentrations on Renca cells when cultured with CAFs-CM (the absorbance of sunitinib at a concentration of 0 μM was used as control in both the CAFs-CM group and NFs-CM group.

(D) Transwell migration and invasion of Renca cells after 36 h treatment.

Figure 2. Continued

(E) Wound healing and closure rate of Renca cells. NFs-CM represents a 1:1 mixture of NIH-3T3 conditioned medium and fresh culture medium, wherein CAFs-CM represents a 1:1 mixture of mouse-derived CAFs conditioned medium and fresh culture medium.

(F–H) Tumor morphology, tumor volume curve, and tumor weight in tumor bearing mice.

(I and J) Representative morphology and H&E staining of lung tissues. (I) and (J) share control and Co-CAFs group with that in Figure S10D. Scale bar: 100 μm. Data are shown as mean ± SEM, n = 3∼6, *p < 0.05, **p < 0.01, ***p < 0.001, ns: no significance.

LOXL1, and *LUM*[21] exhibited significantly lower survival probabilities (Figure S2). Immunofluorescence staining indicated that the expression of alpha-smooth muscle actin (a-SMA), fibroblast specific protein 1 (FSP1), fibroblast activating protein (FAP), and vimentin in tumor sites were elevated (Figure S3). Collectively, these findings underscore the CAFs infiltration in RCC tissues.

We then isolated and identified CAFs and NFs from patient tumor tissues and tumor-adjacent tissues separately according to established methods (Figure S4). As shown in Figures 1A and 1B, CAFs-CM significantly increased the proliferation of ACHN and 786-O cells. Importantly, tumor cells cultured with CAFs-CM showed strengthened sunitinib resistance, whereas no comparable outcomes were observed in NFs-CM group (Figures 1C and 1D). Additionally, ACHN and 786-O cells cultured with CAFs-CM exhibited enhanced migration and invasion ability (Figures 1E and 1F). The wound healing assay also indicated that CAFs-CM could promote the wound closure in ACHN and 786-O cells (Figures 1G and 1H). These results suggest that patient-derived CAFs could augment RCC cells proliferation, migration, and resistance to sunitinib, likely through the secretion of soluble factors.

CAFs obtained from xenograft tumors promoted the progression and sunitinib resistance of RCC

Xenograft tumor-derived CAFs were isolated from tumor-bearing BALB/C mice (Figure S5). NIH-3T3 cells were used as NFs control. According to Figures 2A and 2B, CAFs-CM significantly increased the proliferation and colony formation of Renca cells *in vitro*. Moreover, sunitinib typically inhibited Renca cell proliferation in a dose-dependent manner, the presence of CAFs-CM was found to counteract this effect, particularly at higher concentrations (Figure 2C). This suggests a pronounced role of CAFs-CM in sunitinib resistance. Furthermore, we also found that CAFs-CM enhanced wound healing, migration, and invasion of Renca cells (Figures 2D and 2E). The *in vivo* results showed that sunitinib significantly inhibited tumor proliferation, reducing tumor volume and tumor weight. Additionally, co-transplantation with CAFs not only increased tumor volume and tumor weight but also diminished the therapeutic effects of sunitinib, underscoring the influential role of CAFs in tumor growth and drug resistance (Figures 2F–2H and S6). Furthermore, the co-transplantation with CAFs significantly enhanced lung metastasis of Renca cells (Figures 2I and 2J), highlighting the metastatic potential driven by CAFs. These results suggest that xenograft tumor-derived CAFs promoted the progression and sunitinib resistance of RCC both *in vivo* and *in vitro*.

Identification of CAFs-derived CXCL3 as a potential mediator in RCC progression

All these aforementioned results indicated that some soluble factors secreted by CAFs may be accountable for promoting tumor cell growth and drug resistance. Exposure of CAFs-CM to heat eliminated the effect of CAFs-CM on Renca cells, implicating proteins as the likely active components facilitating tumor enhancement (Figures 3A–3C). To further investigate the mechanism by which CAFs promote the progression and drug resistance in RCC, label-free proteomics sequencing was performed to compare the different secreted proteins between the serum-free medium of CAFs (obtained from xenograft tumors) and NFs (NIH-3T3). We found that the secretion of 115 proteins significantly increased in CAFs serum-free conditioned medium (Figures 3D and 3E). CXCL3 emerged as a candidate of interest for further investigation based on preliminary results. ELISA assays confirmed significantly higher levels of CXCL3 in CAFs-CM compared to NFs-CM (Figure 3F). Moreover, gene expression analysis showed elevated *CXCL3* levels in human CAFs and patient tumor tissues, as opposed to NFs or tumor-adjacent tissues (Figures 3G, 3H, and S7A). Co-transplantation with CAFs subcutaneously further upregulated CXCL3 expression in tumor tissues (Figure 3I). Crucially, *CXCL3* expression was negatively correlated with survival probability among RCC patients (Figure S7B), positioning CXCL3 not only as a mediator of tumor progression and drug resistance but also as a potential predictive biomarker for RCC prognosis.

CAFs promoted RCC progression and sunitinib resistance through CXCL3/CXCR2

To further clarify the effect of CXCL3 on tumor cells, we stimulated Renca cells with exogenous CXCL3. As shown in Figure 4A, CXCL3 could promote tumor proliferation in a gradient manner. The most significant effect was observed at a concentration of 10 ng/mL. This optimal concentration was chosen for further experiments, which confirmed that CXCL3 notably enhanced the migration and invasion capabilities of Renca cells (Figure 4B). Additionally, CXCL3 exposure reduced RCC cells' sensitivity to sunitinib, underscoring its role in drug resistance (Figure 4C). Utilizing small interfering RNA (siRNA) to knock down CXCL3 expression in CAFs resulted in a marked decrease in CXCL3 levels, with siCXCL3-283 being the most effective (Figures S8A and S8B). This knockdown significantly mitigated the CAFs-induced effects on Renca cell proliferation, migration, and sunitinib resistance (Figures 4D–4F). Conversely, overexpressing *Cxcl3* in NIH3T3cells endowed its pro-proliferative and pro-drug resistance effects on Renca cells (Figures 4G, 4H, S8C, and S8D).

CXCL3 activates its receptor CXCR2 to triggers the downstream signaling pathways.[22] Further experiments highlighted the CXCL3/CXCR2 pathway's central role, with increased CXCR2 expression in RCC tissues and enhanced expression following co-transplantation with CAFs (Figures S9A and S9B). The effects of CAFs-CM or CXCL3 on CXCR2 expression was not be detected by flow cytometry. However, both CAFs-CM and CXCL3 treatment upregulated the gene or protein expression of CXCR2 in Renca cells (Figures S9C–S9F). Therefore,
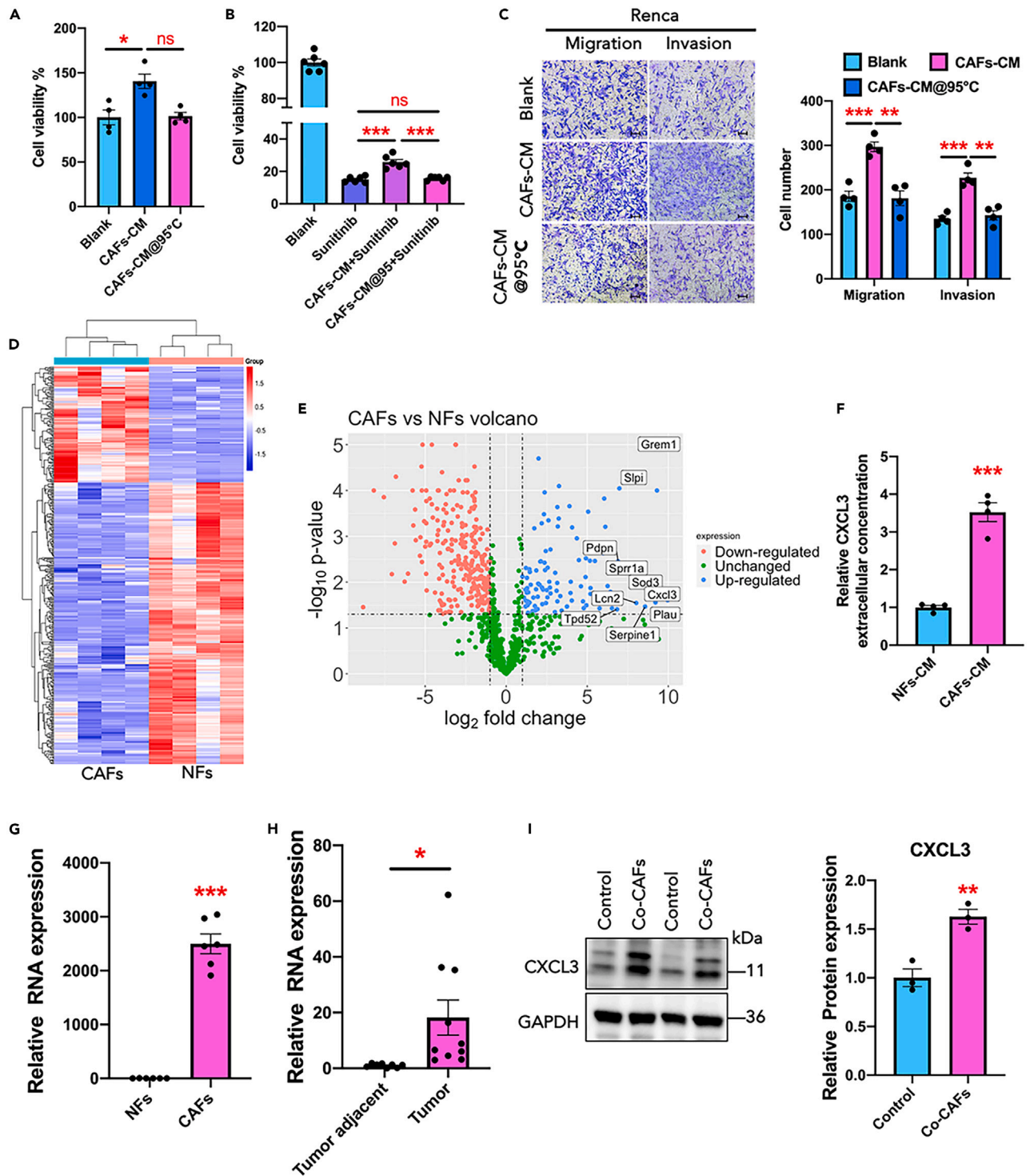
Figure 3. CAFs-derived CXCL3 acted as a potential mediator in RCC progression

(A) Cell viability% of Renca cells cultured with heated CAFs-CM.

(B) The cytotoxicity of sunitinib at different concentrations on Renca co-cultured with heated CAFs-CM.

(C) Crystal violet staining and quantification of migrated and invasive Renca cells after 36 h treatment.

(D) Proteomics sequencing clustering analysis of mouse-derived CAFs serum-free conditioned medium (CAFs) and NIH-3T3 serum-free conditioned medium (NFs).

(E) Differential protein volcano map of CAFs versus NFs serum-free conditioned medium.

Figure 3. *Continued*
(F) CXCL3 concentration in the CAFs and NFs conditioned medium.
(G) Gene expression of *Cxcl3* in CAFs and NFs.
(H) Gene expression of *CXCL3* in RCC tissue.
(I) Protein expression of CXCL3 in tumor tissue of tumor-bearing mice. Scale bar: 100 μm. Data are shown as mean ± SD in (D) and (E), mean ± SEM in other panels, $n = 3\sim6$, $*p < 0.05$, $**p < 0.01$, $***p < 0.001$, ns: no significance.

CXCR2 antagonist SB225002 was used to block the interaction between CAFs-CM and tumor cells. Our results showed that SB225002 could inhibit the expression of *Cxcr2* in Renca cells (Figure S9G). Although the number of CAFs was not being affected by CXCR2 inhibition, SB225002 further reversed the pro-tumorigenic effects of CAFs both *in vivo* and *in vitro* (Figures 4I–4K and S10) confirming the critical role of the CXCL3/CXCR2 pathway in mediating CAFs' effects on RCC progression. All the aforementioned results indicated that CAFs may promote RCC tumor progression through CXCL3/CXCR2.

CAFs and CXCL3 activated ERK1/2 signaling pathway in RCC

As a downstream pathway of CXCR2, ERK1/2 signaling is activated by CXCR2 ligand binding, and affects epithelial mesenchymal transformation (EMT) and tumor cell stemness.[23] The gene set enrichment analysis (GSEA) results demonstrated significant enrichment for the ERK signaling pathway with high CXCL3 expression (Figure S11A), indicating a strong relationship between CXCL3 and ERK signaling activation in RCC. Experimental validation showed that both CAFs-CM and exogenous CXCL3 substantially increased ERK1/2 phosphorylation in Renca cells (Figures 5A and 5B). Notably, the effect of CAFs-CM on ERK1/2 phosphorylation was negated by CXCL3 knockdown using siRNA (Figure 5C), while the CXCR2 antagonist SB225002 inhibited further ERK1/2 activation induced by CAFs-CM or CXCL3 (Figures S11B and S11C). Moreover, co-transplantation with CAFs led to enhanced ERK1/2 activation in mouse tumor tissues (Figure 5D). CAFs-CM and CXCL3 increased the protein expression of CD133 and gene expression of stemness related genes (*Cd44*, *Nanog*, *Aldh1a1*, or *Sox2*) in Renca cells (Figures 5E, 5F, S12A, and S12B), indicating their potential role in promoting tumor cell stemness. Additionally, CAFs-CM and CXCL3 increased the protein expression of N-cadherin and enhanced the EMT phenotype of Renca cells (Figures 5E, 5F, and S12C), affecting the EMT process. Meanwhile, Co-CAFs transplantation facilitated the stemness and EMT maintenance in mice tumor tissues (Figure 5G), which may be one of the reasons for the enhanced tumor progression and drug resistance.

Tumor cells promoted the transformation of NFs into CAFs and the expression of CXCL3 in fibroblasts

Bioinformatics analysis of the The Cancer Genome Atlas (TCGA) database highlighted a significant increase in *Tgf-β* expression in RCC tissues compared to normal tissues (Figure S13A), suggesting TGF-β's involvement in RCC. Furthermore, GSEA underscored a strong association between *CXCL3* expression and TGF-β signaling pathway activation in RCC (Figure S13B). As shown in Figures 6A and 6B, Renca cell-conditioned medium (Renca-CM) significantly increased the expression of CAF-signature genes (*α-Sma*, *Fsp1*, *vimentin*, or *Fap*) in NIH-3T3 cells or MEF, indicating a potentiation of NFs to CAFs transformation. Renca-CM also induced a marked increase in *Cxcl3* expression in both NIH-3T3 and MEF (Figures 6C and 6D). Although the effects on traditional CAF-signatures were less pronounced (Figure 6E), *Cxcl3* expression was significantly elevated in CAFs treated with Renca-CM (Figure 6F). The conditioned medium form transformed NIH-3T3 and MEF cells facilitated the proliferation and sunitinib resistance of Renca cells *in vitro* (Figures 6G–6J). Meanwhile, transformed MEF promoted the progression, lung metastasis, and sunitinib resistance *in vivo* (Figures 6K–6N), further illustrating the significant role of induced CAFs in RCC pathogenesis.

Renca cells promoted the transformation and CXCL3 expression of fibroblasts through TGF-β-Smad2/3 signaling pathway

CAFs-CM and CXCL3 induced a notable upregulation in the expression of *Tgf-β* in Renca tumor cells (Figures 7A–7C). In response to TGF-β stimulation, NIH-3T3 and MEF could transform into CAFs, as evidenced by the upregulation of key genes such as *Fsp1*, *Fap*, and *vimentin* (Figures S14A and S14B). This transformation was accompanied by a significant increase in *CXCL3* expression in both NIH-3T3 and MEF cells. Although direct TGF-β stimulation did not induce further transformation in CAFs, it notably enhanced *CXCL3* expression (Figure S14C). Knockdown of TGF-β expression in Renca cells using siRNA (Figures 7D and 7E) resulted in impaired ability of Renca-CM to promote *Cxcl3* expression in fibroblasts (Figures 7F and 7G) highlighting TGF-β's critical role in this process. Moreover, investigations into the Smad2/3 pathway activation revealed that both TGF-β and Renca-CM significantly induced the phosphorylation of Smad2 and Smad3 in NIH-3T3 cells (Figures 7H and 7I), suggesting that TGF-β-Smad2/3 signaling may be a key mechanism through which Renca-CM promotes NFs transformation into CAFs and enhances CXCL3 secretion.

DISCUSSION

Microenvironmental factors have been identified as additional contributors to RCC progression and drug resistance.[24–26] The dynamic interplay between CAFs and cancer cells hinges on a multitude of molecular mechanisms. Our study explored the complex terrain of RCC progression, underscoring the pivotal role of microenvironmental factors, with a particular focus on the dynamic interplay between CAFs and cancer cells. Through a series of rigorous analyses, we have illuminated the critical function of the CXCL3/TGF-β paracrine signaling axis in mediating direct crosstalk between CAFs and tumor cells.
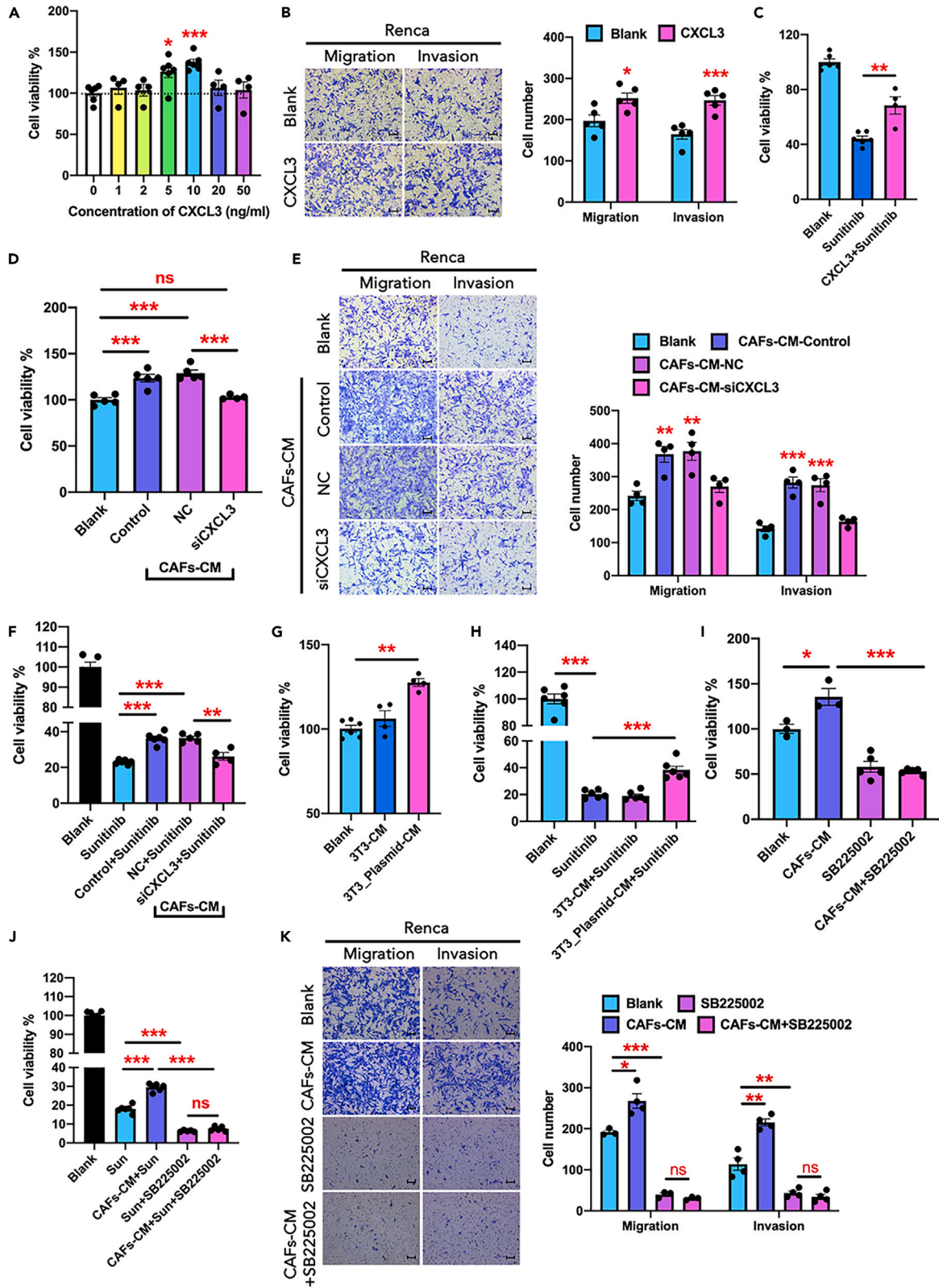
Figure 4. CAFs promoted RCC progression and sunitinib resistance through CXCL3/CXCR2

(A) Renca mean ± cell viability% of Renca cells was evaluated by the CCK8 assay after stimulation with different doses of CXCL3 (0.5, 1, 2, 5, 10, 20, and 50 ng/mL) for 24 h.

(B) Crystal violet staining and quantification of migrated Renca cells after CXCL3 treatment for 36 h.

(C) Sunitinib cytotoxicity at a concentration of 20 μM in Renca cells with or without CXCL3 stimulation.

(D) Cell viability of Renca cells co-cultured with conditioned medium from CAFs with CXCL3 interference.

(E) Transwell migration or invasion and their quantifications of Renca cells stimulated by CXCL3-interfering CAFs-CM.

(F) Sunitinib (20 μM) cytotoxicity of Renca cells co-cultured with CAFs-CM-siCXCL3.

(G and H) Cell viability and sunitinib cytotoxicity of Renca cells co-cultured with conditioned medium from CXCL3 overexpressed NIH3T3cells.

(I–K) The effects of SB225002 on the proliferation, migration and sunitinib resistance of Renca cells induced by CAFs-CM. Scale bar: 100 μm. Data are shown as mean ± SEM, $n = 3\sim6$, $*p < 0.05$, $**p < 0.01$, $***p < 0.001$, ns: no significance.

Previous studies have demonstrated that CAFs are essential for the occurrence and progression of renal carcinoma.[27] In recurrent RCC, a significant correlation has been found between $CD8^+T$ cell reduction and CAFs infiltration, which contributes to adverse immunotherapy reactions.[28] Furthermore, non-coding RNA delivered by exosomes from CAFs promotes the progression of RCC.[29,30] In this study, we found that the infiltration of CAFs in RCC tissue was increased, which was verified by immunofluorescence staining. Additionally, the CAFs isolated from patients and tumor-bearing mice promoted the progression of RCC and the resistance to sunitinib, consistent with the previous reports.

Increasing research has revealed the correlation between CXCL3 and various types of tumors.[31] Our proteomics analysis indicated that the expression of CXCL1, CXCL3, and CXCL5 in CAFs serum-free medium was higher than that in NFs, with CXCL3 showing the most significant difference. These results confirmed that exogenous CXCL3 could promote the proliferation, migration, and resistance to sunitinib in RCC cells. Interference of *CXCL3* expression by siRNA reversed the effect of CAFs on tumor progression, while overexpression of *CXCL3* promoted the proliferation and sunitinib resistance, further proved its importance in RCC progression.

As a receptor of CXCL3, CXCR2 activation increased the phosphorylation-mediated activation of pathways such as Raf-MEK-ERK, which further promoted tumor progression through a downstream cascade.[13–15] In this study, the GSEA analysis based on TCGA database suggested a positive correlation between the ERK pathway and CXCL3 expression. We found that CAFs-CM and CXCL3 could promote the phosphorylation of ERK1/2. Moreover, CAFs-CM and CXCL3 could upregulate the expression of N-cadherin and CD133, suggesting that CAFs-CM and CXCL3 may facilitate the EMT and cell stemness of tumors, which related to tumor metastasis and drug resistance.

It was reported a significant inhibition of Renca tumor growth was found in CXCR2 knockout mice, and the potential of *in situ* Renca tumors to metastasize to the lung was reduced in the absence of CXCR2,[16] indicating that ligands of CXCR2 might be involved in the progression of RCC. In addition to CXCL3, other CXCR2 ligands were identified based on proteomics, such as CXCL1 and CXCL5, which have been reported to be secreted by CAFs in other tumors, promoting tumor progression through CXCR2. Additionally, both CXCL8[32,33] and CXCL2[34] have important roles in the development of tumors, which are all the ligands of CXCR2. He et al.[31] used CXCL3 neutralizing antibody to inhibit the migration and invasion of breast cancer cells, but did not investigate its effect on tumor progression *in vivo*; instead, CXCR2 non-peptide antagonist SB225002 was used for combined administration. Combined treatment with CXCR2 inhibitors can inhibit tumor progression and avoid chemotherapy resistance,[35] and corresponding phase II clinical studies on CXCR2 inhibitors are also being carried out (NCT03177187 and NCT02583477). In our study, a selective and non-peptide CXCR2 antagonist SB225002 was chosen to block CXCL/CXCR2 interaction. The *in vitro* and *in vivo* results highlighted the antagonistic effects of SB225002 on the progression and sunitinib resistance of RCC.

Moreover, tumor cells were reported to encourage the conversion of NFs into CAFs through paracrine factors,[17,18] further promoting tumor progression through a positive feedback pathway. Thus, the interaction among CAFs and tumor cells were explored in our study. We have observed that Renca cells promoted the transformation of NFs into the CAFs phenotype and induced the secretion of CXCL3 through the TGF-β-Smad2/3 signaling pathway. Notably, CAFs signatures were upregulated in NIH-3T3 and MEF cells after stimulation with Renca-CM or TGF-β. Conversely, no substantial changes in marker genes were observed when CAFs themselves were stimulated. This discrepancy may be attributed to the inherently elevated expression levels of these genes in CAFs. However, CAFs engage in intricate interactions not only with tumor cells but also with tumor-infiltrating immune cells and other immune components within the TME. These interactions involve the secretion of a myriad of cytokines, growth factors, chemokines, exosomes, and other effector molecules, thereby shaping an immunosuppressive TME that confers cancer cells with the ability to evade immune system surveillance.[36]

Limitations of the study

Our study demonstrated the role of CAFs in promoting the progression of RCC through the CXCL3/TGF-β mediated cellular crosstalk. However, the involvement of additional cytokines and cell-cell interactions remains unknown. Furthermore, it is crucial to acknowledge that alternative mechanisms through which CAFs exert their influence on RCC progression and drug resistance cannot be discounted.[30,37] In addition, the heterogeneity of CAFs has been proposed,[38,39] which suggests a need for further research into the classification of CAFs subtypes.

STAR★METHODS

Detailed methods are provided in the online version of this paper and include the following:

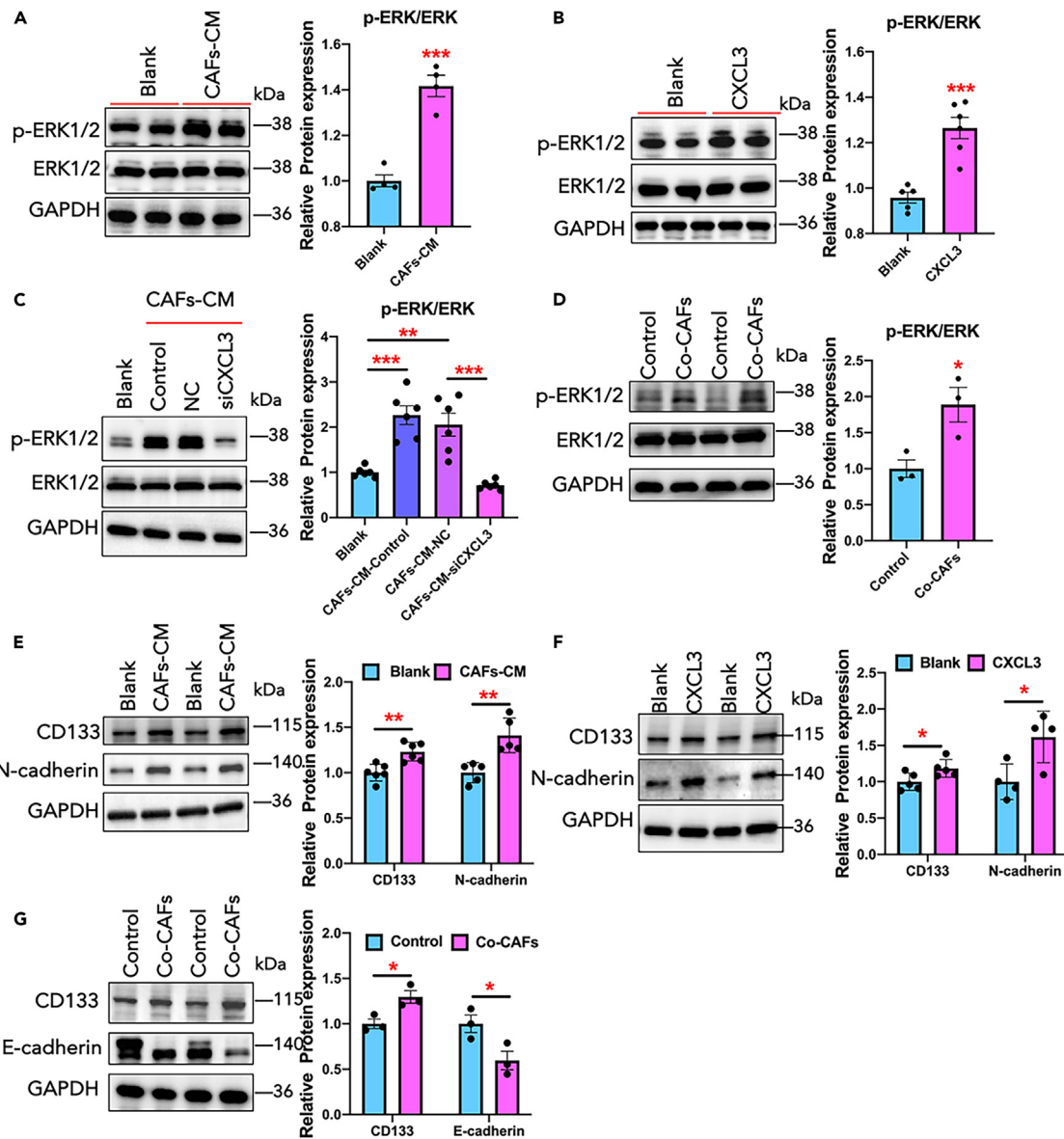- KEY RESOURCES TABLE
- RESOURCE AVAILABILITY

Figure 5. CAFs-CM and CXCL3 regulated ERK1/2 signaling pathway

(A and B) Western blot analysis and quantification of ERK1/2 and phosphorylated-ERK1/2 expression in Renca cells stimulated with CAFs-CM or CXCL3.

(C) Expression of ERK1/2 and phosphorylated-ERK1/2 in Renca cells stimulated with conditioned medium from CAFs with CXCL3 interference.

(D) Protein expression of ERK1/2 and phosphorylated-ERK1/2 in tumor tissue of tumor-bearing mice.

(E and F) Protein expression of N-cadherin and CD133 in Renca cells stimulated with CAFs-CM or CXCL3.

(G) Protein expression of CD133 and E-cadherin in tumor tissue of tumor-bearing mice. Data are shown as mean $\pm$ SEM, n = 3~6, *p < 0.05, **p < 0.01, ***p < 0.001.

- ○ Lead contact
- ○ Materials availability
- ○ Data and code availability
- ● EXPERIMENTAL MODEL AND STUDY PARTICIPANT DETAILS
  - ○ Ethics statement
- ● METHOD DETAILS
  - ○ Cell proliferation and cytotoxicity assay
  - ○ Invasion and migration assays

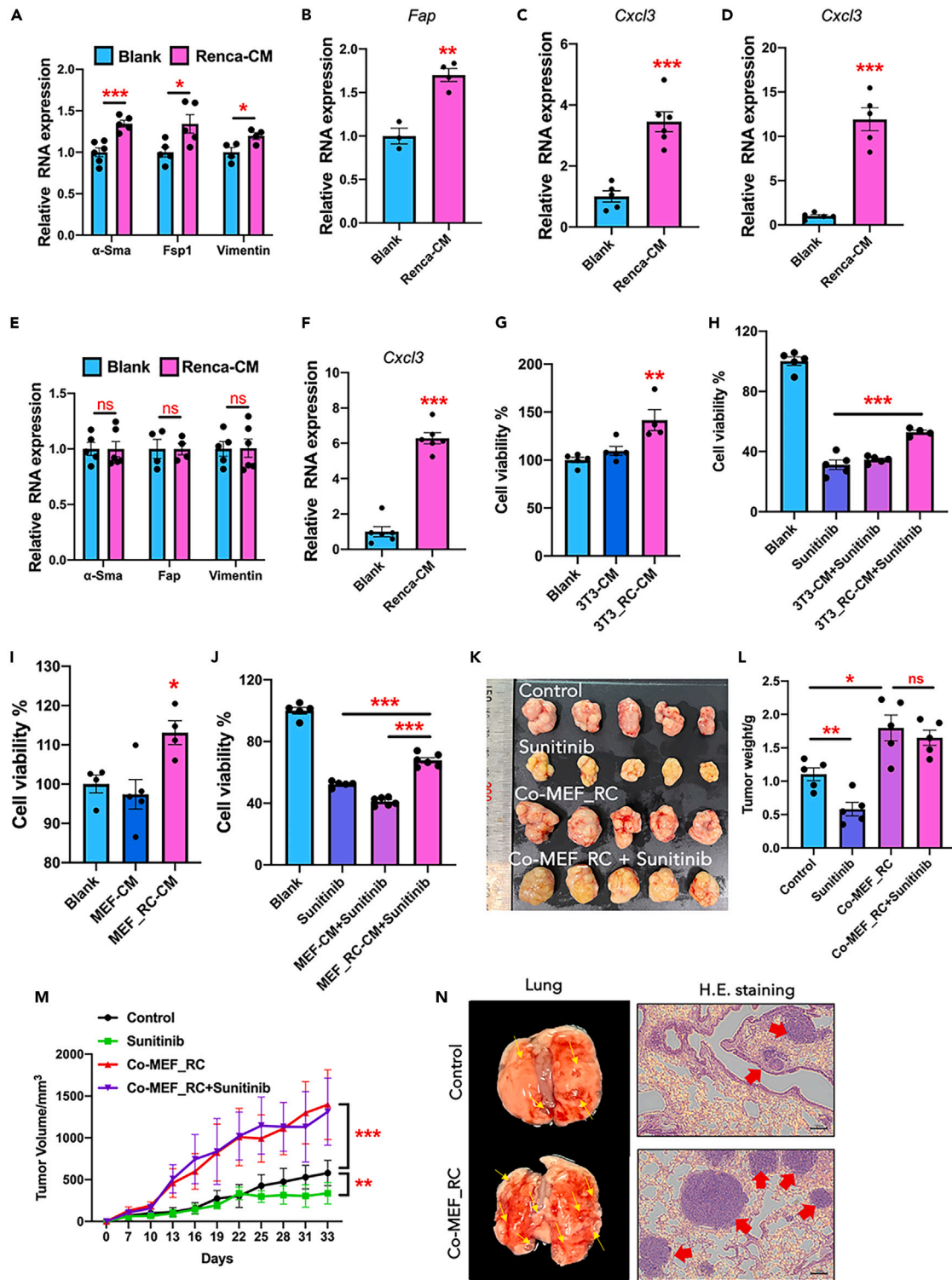**Figure 6. Tumor cells promoted the transformation of NFs into CAFs**

(A) The gene expression of *α-Sma*, *Fsp1*, and *vimentin* in NIH3T3cells stimulated by Renca-CM.

(B) The gene expression of *Fap* in MEF stimulated by Renca-CM.

(C and D) The gene expression of *Cxcl3* in NIH-3T3 and MEF cells treated with Renca-CM.

(E) The gene expression of *α-Sma*, *Fap*, and *vimentin* in CAFs stimulated by Renca-CM.

Figure 6. Continued

(F) The gene expression of *Cxcl3* in CAFs treated with Renca-CM.

(G and H) Cell viability and sunitinib cytotoxicity of Renca cells co-cultured with conditioned medium from transformed NIH3T3cells.

(I and J) Cell viability and sunitinib cytotoxicity of Renca cells co-cultured with conditioned medium from transformed MEF cells.

(K–M) Tumor morphology, tumor volume curve, and tumor weight in tumor bearing mice co-transplanted with transformed MEF.

(N) Representative morphology and H&E staining of lung tissues co-injected with transformed MEF. Scale bar: 100 μm. Data are shown as mean $\pm$ SEM in experiments, $n = 3\sim5$, $*p < 0.05$, $**p < 0.01$, $***p < 0.001$.

- ○ Wound healing
- ○ Colony formation
- ○ Plasmid or small interfering RNA transfection
- ○ Real-time PCR analysis
- ○ Western blot analysis
- ○ Label-free proteomics sequencing
- ○ Flow cytometry
- ○ The Cancer Genome Atlas data analysis
- ● QUANTIFICATION AND STATISTICAL ANALYSIS

SUPPLEMENTAL INFORMATION

Supplemental information can be found online at https://doi.org/10.1016/j.isci.2024.110224.

AUTHOR CONTRIBUTIONS

All authors contributed extensively to the work presented in this paper. Y.G. and W.C. designed this project, Y.W. and W.D. performed the experiments and wrote up the manuscript. W.H., L.G., J.Z., and Z.Q. provided help for the laboratory technique, experiments, and data analysis. Y.P. helped with bioinformatics analysis. W.D. and K.X. collected human samples and modified the manuscript. All authors contributed to the general discussion. All authors read and approved the final manuscript.

DECLARATION OF INTERESTS

The authors declare no competing interests.

REFERENCES

1. Siegel, R.L., Miller, K.D., Wagle, N.S., and Jemal, A. (2023). Cancer statistics, 2023. CA. Cancer J. Clin. *73*, 17–48. https://doi.org/10.3322/caac.21763.

2. Bukavina, L., Bensalah, K., Bray, F., Carlo, M., Challacombe, B., Karam, J.A., Kassouf, W., Mitchell, T., Montironi, R., O'Brien, T., et al. (2022). Epidemiology of Renal Cell Carcinoma: 2022 Update. Eur. Urol. *82*, 529–542. https://doi.org/10.1016/j.eururo.2022.08.019.

3. Xiao, Y., and Yu, D. (2021). Tumor microenvironment as a therapeutic target in cancer. Pharmacol. Ther. *221*, 107753. https://doi.org/10.1016/j.pharmthera.2020.107753.

4. Anderson, N.M., and Simon, M.C. (2020). The tumor microenvironment. Curr. Biol. *30*. R921–r925. https://doi.org/10.1016/j.cub.2020.06.081.

5. Chen, X., and Song, E. (2019). Turning foes to friends: targeting cancer-associated fibroblasts. Nat. Rev. Drug Discov. *18*, 99–115. https://doi.org/10.1038/s41573-018-0004-1.

6. Biffi, G., and Tuveson, D.A. (2021). Diversity and Biology of Cancer-Associated Fibroblasts. Physiol. Rev. *101*, 147–176. https://doi.org/10.1152/physrev.00048.2019.

7. Sahai, E., Astsaturov, I., Cukierman, E., DeNardo, D.G., Egeblad, M., Evans, R.M., Fearon, D., Greten, F.R., Hingorani, S.R., Hunter, T., et al. (2020). A framework for advancing our understanding of cancer-associated fibroblasts. Nat. Rev. Cancer *20*, 174–186. https://doi.org/10.1038/s41568-019-0238-1.

8. D'Arcangelo, E., Wu, N.C., Cadavid, J.L., and McGuigan, A.P. (2020). The life cycle of cancer-associated fibroblasts within the tumour stroma and its importance in disease outcome. Br. J. Cancer *122*, 931–942. https://doi.org/10.1038/s41416-019-0705-1.

9. Sun, X., He, X., Zhang, Y., Hosaka, K., Andersson, P., Wu, J., Wu, J., Jing, X., Du, Q., Hui, X., et al. (2022). Inflammatory cell-derived CXCL3 promotes pancreatic cancer metastasis through a novel myofibroblast-hijacked cancer escape mechanism. Gut *71*, 129–147. https://doi.org/10.1136/gutjnl-2020-322744.

10. Xin, H., Cao, Y., Shao, M.L., Zhang, W., Zhang, C.B., Wang, J.T., Liang, L.C., Shao, W.W., Qi, Y.L., Li, Y., et al. (2018). Chemokine CXCL3 mediates prostate cancer cells proliferation, migration and gene expression changes in an autocrine/paracrine fashion. Int. Urol. Nephrol. *50*, 861–868. https://doi.org/10.1007/s11255-018-1818-9.

11. Zhou, C., He, X., Tong, C., Li, H., Xie, C., Wu, Y., Wang, L., Yan, X., Luo, D., Tang, Y., et al. (2022). Cancer-associated adipocytes promote the invasion and metastasis in breast cancer through LIF/CXCLs positive feedback loop. Int. J. Biol. Sci. *18*, 1363–1380. https://doi.org/10.7150/ijbs.65227.
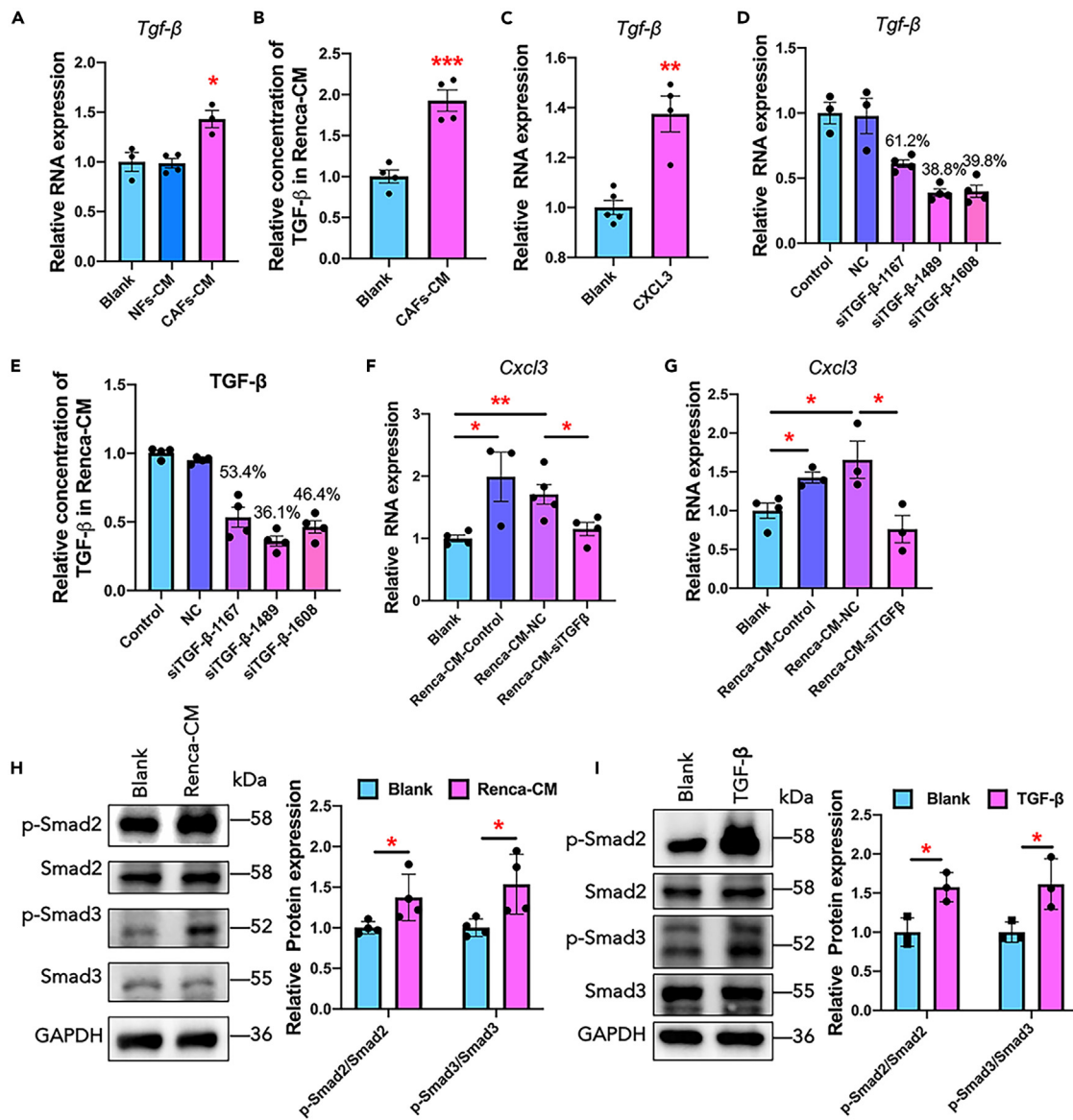
Figure 7. Renca cells promoted the transformation and CXCL3 expression of fibroblasts through TGF-β-Smad2/3 signaling pathway

(A and B) The gene expression and extracellular secretion of TGF-β in Renca cells following treatment with CAFs-CM.

(C) The gene expression of *Tgf-β* in Renca cells treated by CXCL3.

(D and E) The gene expression and extracellular secretion of TGF-β in Renca cells interfered with siRNA.

(F and G) The *Cxcl3* expression in NIH3T3cells or CAFs co-cultured with conditioned medium from Renca cells with TGF-β interference, respectively.

(H and I) The protein expression of Smad2/3, and phosphorylated-Smad2/3 in NIH3T3cells treated by TGF-β and Renca-CM, along with their quantification. Data are shown as mean ± SEM, n = 3∼5, *p < 0.05, **p < 0.01, ***p < 0.001.

12. Wang, H., Zhang, B., Li, R., Chen, J., Xu, G., Zhu, Y., Li, J., Liang, Q., Hua, Q., Wang, L., et al. (2022). KIAA1199 drives immune suppression to promote colorectal cancer liver metastasis by modulating neutrophil infiltration. Hepatology *76*, 967–981. https://doi.org/10.1002/hep.32383.

13. Ma, X., Liu, J., Yang, X., Fang, K., Zheng, P., Liang, X., and Liu, J. (2020). Mesenchymal stem cells maintain the stemness of colon cancer stem cells via interleukin-8/mitogen-activated protein kinase signaling pathway.

Exp. Biol. Med. *245*, 562–575. https://doi.org/10.1177/1535370220910690.

14. Sun, Q., Sun, F., Wang, B., Liu, S., Niu, W., Liu, E., Peng, C., Wang, J., Gao, H., Liang, B., et al. (2014). Interleukin-8 promotes cell migration through integrin αvβ6 upregulation in colorectal cancer. Cancer Lett. *354*, 245–253. https://doi.org/10.1016/j.canlet.2014.08.021.

15. Ha, H., Debnath, B., and Neamati, N. (2017). Role of the CXCL8-CXCR1/2 Axis in Cancer and Inflammatory Diseases. Theranostics *7*,

1543–1588. https://doi.org/10.7150/thno.15625.

16. Mestas, J., Burdick, M.D., Reckamp, K., Pantuck, A., Figlin, R.A., and Strieter, R.M. (2005). The role of CXCR2/CXCR2 ligand biological axis in renal cell carcinoma. J. Immunol. *175*, 5351–5357. https://doi.org/10.4049/jimmunol.175.8.5351.

17. Erez, N., Truitt, M., Olson, P., Arron, S.T., and Hanahan, D. (2010). Cancer-Associated Fibroblasts Are Activated in Incipient Neoplasia to Orchestrate Tumor-Promoting

Inflammation in an NF-kappaB-Dependent Manner. Cancer Cell *17*, 135–147. https://doi.org/10.1016/j.ccr.2009.12.041.

18. Sharon, Y., Raz, Y., Cohen, N., Ben-Shmuel, A., Schwartz, H., Geiger, T., and Erez, N. (2015). Tumor-derived osteopontin reprograms normal mammary fibroblasts to promote inflammation and tumor growth in breast cancer. Cancer Res. *75*, 963–973. https://doi.org/10.1158/0008-5472.Can-14-1990.

19. Ringuette Goulet, C., Bernard, G., Tremblay, S., Chabaud, S., Bolduc, T., and Pouliot, F. (2018). Exosomes Induce Fibroblast Differentiation into Cancer-Associated Fibroblasts through TGFβ Signaling. Mol. Cancer Res. *16*, 1196–1204. https://doi.org/10.1158/1541-7786.Mcr-17-0784.

20. Wu, F., Yang, J., Liu, J., Wang, Y., Mu, J., Zeng, Q., Deng, S., and Zhou, H. (2021). Signaling pathways in cancer-associated fibroblasts and targeted therapy for cancer. Signal Transduct. Target. Ther. *6*, 218. https://doi.org/10.1038/s41392-021-00641-0.

21. Liu, B., Chen, X., Zhan, Y., Wu, B., and Pan, S. (2020). Identification of a Gene Signature for Renal Cell Carcinoma-Associated Fibroblasts Mediating Cancer Progression and Affecting Prognosis. Front. Cell Dev. Biol. *8*, 604627. https://doi.org/10.3389/fcell.2020.604627.

22. Al-Alwan, L.A., Chang, Y., Mogas, A., Halayko, A.J., Baglole, C.J., Martin, J.G., Rousseau, S., Eidelman, D.H., and Hamid, Q. (2013). Differential roles of CXCL2 and CXCL3 and their receptors in regulating normal and asthmatic airway smooth muscle cell migration. J. Immunol. *191*, 2731–2741. https://doi.org/10.4049/jimmunol.1203421.

23. Hsu, Y.L., Hou, M.F., Kuo, P.L., Huang, Y.F., and Tsai, E.M. (2013). Breast tumor-associated osteoblast-derived CXCL5 increases cancer progression by ERK/MSK1/Elk-1/snail signaling pathway. Oncogene *32*, 4436–4447. https://doi.org/10.1038/onc.2012.444.

24. Zhang, Y., Narayanan, S.P., Mannan, R., Raskind, G., Wang, X., Vats, P., Su, F., Hosseini, N., Cao, X., Kumar-Sinha, C., et al. (2021). Single-cell analyses of renal cell cancers reveal insights into tumor microenvironment, cell of origin, and therapy response. Proc. Natl. Acad. Sci. USA *118*, e2103240118. https://doi.org/10.1073/pnas.2103240118.

25. Lai, Y., Tang, F., Huang, Y., He, C., Chen, C., Zhao, J., Wu, W., and He, Z. (2021). The tumour microenvironment and metabolism in renal cell carcinoma targeted or immune therapy. J. Cell. Physiol. *236*, 1616–1627. https://doi.org/10.1002/jcp.29969.

26. Zhang, Z., Karthaus, W.R., Lee, Y.S., Gao, V.R., Wu, C., Russo, J.W., Liu, M., Mota, J.M., Abida, W., Linton, E., et al. (2020). Tumor Microenvironment-Derived NRG1 Promotes Antiandrogen Resistance in Prostate Cancer. Cancer Cell *38*, 279–296.e9. https://doi.org/10.1016/j.ccell.2020.06.005.

27. Zhang, S., Zhou, C., Zhang, D., Huang, Z., and Zhang, G. (2019). The anti-apoptotic effect on cancer-associated fibroblasts of B7-H3 molecule enhancing the cell invasion and metastasis in renal cancer. OncoTargets Ther. *12*, 4119–4127. https://doi.org/10.2147/ott.S201121.

28. Peng, Y.L., Xiong, L.B., Zhou, Z.H., Ning, K., Li, Z., Wu, Z.S., Deng, M.H., Wei, W.S., Wang, N., Zou, X.P., et al. (2022). Single-cell transcriptomics reveals a low CD8$^+$ T cell infiltrating state mediated by fibroblasts in recurrent renal cell carcinoma. J. Immunother. Cancer *10*, e004206. https://doi.org/10.1136/jitc-2021-004206.

29. Liu, Y., Fu, W., Cao, X., Li, S., Xiong, T., Zhang, X., Wu, X., Cheng, L., Wei, Y., and Gao, B. (2021). Delivery of miR-224-5p by Exosomes from Cancer-Associated Fibroblasts Potentiates Progression of Clear Cell Renal Cell Carcinoma. Comput. Math. Methods Med. *2021*, 5517747. https://doi.org/10.1155/2021/5517747.

30. Ding, M., Zhao, X., Chen, X., Diao, W., Kan, Y., Cao, W., Chen, W., Jiang, B., Qin, H., Gao, J., et al. (2022). Cancer-associated fibroblasts promote the stemness and progression of renal cell carcinoma via exosomal miR-181d-5p. Cell Death Discov. *8*, 439. https://doi.org/10.1038/s41420-022-01219-7.

31. He, X., Wang, L., Li, H., Liu, Y., Tong, C., Xie, C., Yan, X., Luo, D., and Xiong, X. (2023). CSF2 upregulates CXCL3 expression in adipocytes to promote metastasis of breast cancer via the FAK signaling pathway. J. Mol. Cell Biol. *15*, mjad025. https://doi.org/10.1093/jmcb/mjad025.

32. Zhai, J., Shen, J., Xie, G., Wu, J., He, M., Gao, L., Zhang, Y., Yao, X., and Shen, L. (2019). Cancer-associated fibroblasts-derived IL-8 mediates resistance to cisplatin in human gastric cancer. Cancer Lett. *454*, 37–43. https://doi.org/10.1016/j.canlet.2019.04.002.

33. Lopez-Bujanda, Z.A., Haffner, M.C., Chaimowitz, M.G., Chowdhury, N., Venturini, N.J., Patel, R.A., Obradovic, A., Hansen, C.S., Jacków, J., Maynard, J.P., et al. (2021). Castration-mediated IL-8 promotes myeloid infiltration and prostate cancer progression. Nat. Cancer *2*, 803–818. https://doi.org/10.1038/s43018-021-00227-3.

34. Acker, G., Zollfrank, J., Jelgersma, C., Nieminen-Kelhä, M., Kremenetskaia, I., Mueller, S., Ghori, A., Vajkoczy, P., and Brandenburg, S. (2020). The CXCR2/CXCL2 signalling pathway - An alternative therapeutic approach in high-grade glioma. Eur. J. Cancer *126*, 106–115. https://doi.org/10.1016/j.ejca.2019.12.005.

35. Devapatla, B., Sharma, A., and Woo, S. (2015). CXCR2 Inhibition Combined with Sorafenib Improved Antitumor and Antiangiogenic Response in Preclinical Models of Ovarian Cancer. PLoS One *10*, e0139237. https://doi.org/10.1371/journal.pone.0139237.

36. Mao, X., Xu, J., Wang, W., Liang, C., Hua, J., Liu, J., Zhang, B., Meng, Q., Yu, X., and Shi, S. (2021). Crosstalk between cancer-associated fibroblasts and immune cells in the tumor microenvironment: new findings and future perspectives. Mol. Cancer *20*, 131. https://doi.org/10.1186/s12943-021-01428-1.

37. Fu, W., Zhao, H., Liu, Y., Nie, H., Gao, B., Yin, F., Wang, B., Li, T., Zhang, T., Wang, L., et al. (2022). Exosomes Derived from Cancer-Associated Fibroblasts Regulate Cell Progression in Clear-Cell Renal-Cell Carcinoma. Nephron *146*, 383–392. https://doi.org/10.1159/000520304.

38. Geng, X., Chen, H., Zhao, L., Hu, J., Yang, W., Li, G., Cheng, C., Zhao, Z., Zhang, T., Li, L., and Sun, B. (2021). Cancer-Associated Fibroblast (CAF) Heterogeneity and Targeting Therapy of CAFs in Pancreatic Cancer. Front. Cell Dev. Biol. *9*, 655152. https://doi.org/10.3389/fcell.2021.655152.

39. Luo, H., Xia, X., Huang, L.B., An, H., Cao, M., Kim, G.D., Chen, H.N., Zhang, W.H., Shu, Y., Kong, X., et al. (2022). Pan-cancer single-cell analysis reveals the heterogeneity and plasticity of cancer-associated fibroblasts in the tumor microenvironment. Nat. Commun. *13*, 6619. https://doi.org/10.1038/s41467-022-34395-2.

40. Yoshihara, K., Shahmoradgoli, M., Martínez, E., Vegesna, R., Kim, H., Torres-Garcia, W., Treviño, V., Shen, H., Laird, P.W., Levine, D.A., et al. (2013). Inferring tumour purity and stromal and immune cell admixture from expression data. Nat. Commun. *4*, 2612. https://doi.org/10.1038/ncomms3612.

STAR★METHODS

KEY RESOURCES TABLE

REAGENT or RESOURCE	SOURCE	IDENTIFIER
Antibodies		
Rabbit anti-α-SMA Polyclonal Antibody	Proteintech	Cat# 55355-1-AP; RRID:AB_2313773
Rabbit anti-FSP1 Polyclonal Antibody	Proteintech	Cat# 16105-1-AP; RRID:AB_11042591
Rabbit Anti-FAP Rabbit Polyclonal Antibody	Solarbio life science	Cat# K004451P; RRID:AB_2313773
Rabbit Anti-Vimentin Polyclonal Antibody	Proteintech	Cat# 10366-1-AP; RRID: AB_2273020
Rabbit anti-CXCL3 Polyclonal Antibody (GRO gamma Antibody)	Affinity	Cat# DF8554; RRID:AB_2841758
Rabbit anti-CXCR2 Polyclonal Antibody	Proteintech	Cat# 20634-1-AP; RRID:AB_10693624
Rabbit anti-Phospho-ERK1/2 (Thr202/Tyr204) Polyclonal Antibody	Proteintech	Cat# 28733-1-AP; RRID:AB_2881202
Rabbit anti-ERK1/2 Polyclonal Antibody	Proteintech	Cat# 16443-1-AP; RRID:AB_10603369
Rabbit anti-CD133 Polyclonal Antibody	Proteintech	Cat# 18470-1-AP; RRID:AB_2172859
Rabbit anti-N Cadherin Polyclonal Antibody	Boster	Cat# BM3921; RRID:AB_2313773
Rabbit anti-pan-Cadherin Monoclonal Antibody	Boster	Cat# BM4166; RRID:AB_2313773
Rabbit Anti-Phospho SMAD2 (S250)	Boster	Cat# BM4693; RRID:AB_2313773
Phospho-Smad3(Ser423/425)(C25A9)Rabbit mAb	Cell Signaling Technology	Cat# 9520T; RRID:AB_2313773
Mouse Anti-SMAD2 Monoclonal antibody	Proteintech	Cat# 67343-1-Ig; RRID:AB_2313773
Mouse Anti-SMAD3 Monoclonal antibody	Proteintech	Cat# 66516-1-Ig; RRID:AB_2313773
Mouse Anti-GAPDH Monoclonal Antibody	Proteintech	Cat# 60004-1-Ig; RRID:AB_2313773
HRP-conjugated affinipure Goat Anti- Rabbit IgG (H + L)	Proteintech	Cat# SA00001-2; RRID:AB_2722564
HRP-conjugated Affinipure Goat Anti-Mouse IgG (H + L)	Proteintech	Cat# SA00001-1; RRID:AB_2722565
FITC anti-mouse CD182 (CXCR2) Antibody	Biolegend	Cat# 149310; RRID:AB_2566148
Biological samples		
Human renal cell carcinoma tissues	Huashan Hospital, Fudan University	N/A
Chemicals, peptides, and recombinant proteins		
Fetal bovine serum	Gibco	Cat# 16000–044
DMEM medium	Gibco	Cat# C11995500BT
RPMI 1640 medium	Gibco	Cat# C11875500BT
Renca cell culture-medium	Procell	Cat# CM-0568
Penicillin-streptomycin solution	Gibco	Cat# 15140122
CTS™ Opti-MEM™ I	Gibco	Cat# A4124802
Trypsin	Gibco	Cat# 12604021
Recovery Cell Culture Freezing medium	Gibco	Cat# 12648–010
Collagenase A	Roche	Cat# 10103578001
Enhanced Cell Counting Kit-8	Beyotime	Cat# C0043
CXCL3 enzyme-linked immunosorbent assay kit	Elabscience	Cat# E-EL-M0147c
Sunitinib malate	Cayman	Cat# 13159
SB225002	Topscience	Cat# T1955
Recombinant Human GRO-γ (CXCL3)	Cloud-Clone	Cat# RPB604Hu01
Recombinant Human TGF-β1	Peprotech	Cat# 100–21
Lipofectamine™ 3000	Invitrogen	Cat# L3000015
PageRuler Prestained Protein Ladder	Thermo Fisher	Cat# 26616
Total RNA Extraction Reagent	Vazyme	Cat# R401-01

Continued

REAGENT or RESOURCE	SOURCE	IDENTIFIER
Deposited data		
TCGA-KIRC RNA-seq dataset	National Institutes of Health	https://portal.gdc.cancer.gov/projects/TCGA-KIRC
Raw and analyzed data (Label-free proteomics sequencing)	This paper	Mendeley Data: https://data.mendeley.com/datasets/824bwf4hpf/5
Experimental models: Cell lines		
786-O	Procell	Cat# CL-0010; RRID: CVCL_1051
ACHN	Procell	Cat# CL-0021; RRID: CVCL_1067
Renca	Procell	Cat# CL-0568; RRID: CVCL_2174
NIH-3T3	Zhongqiaoxinzhou Biotech	Cat# ZQ0096; RRID: CVCL_0594
Experimental models: Organisms/strains		
Wild type Balb/C mice	Lingchang	N/A
Oligonucleotides		
Cxcl3-mus-254 sense sequence 5′-CACCCAGACAGAAGUCAUAUU-3′	Genepharma	N/A
Cxcl3-mus-254 antisense sequence 5′-UAUGACUUCUGUCUGGGUGUU-3′	Genepharma	N/A
Cxcl3-mus-283 sense sequence 5′-AGGAUGGUCAAGAAGUUUGUU-3′	Genepharma	N/A
Cxcl3-mus-283 antisense sequence 5′-CAAACUUCUUGACCAUCCUUG-3′	Genepharma	N/A
Cxcl3-mus-319 sense sequence 5′-CCAGGCUUCAGAUAAUCAUUU-3′	Genepharma	N/A
Cxcl3-mus-319 antisense sequence 5′-AUGAUUAUCUGAAGCCUGGUU-3′	Genepharma	N/A
Tgfb1-Mus-1608 sense sequence 5′-GCACCAUCCAUGACAUGAAUU-3′	Genepharma	N/A
Tgfb1-Mus-1608 antisense sequence 5′-UUCAUGUCAUGGAUGGUGCUU-3′	Genepharma	N/A
Tgfb1-Mus-1167 sense sequence 5′-CGGACUACUAUGCUAAAGAUU-3′	Genepharma	N/A
Tgfb1-Mus-1167 antisense sequence 5′-UCUUUAGCAUAGUAGUCCGUU-3′	Genepharma	N/A
Tgfb1-Mus-1489 sense sequence 5′-GAACCAAGGAGACGGAAUAUU-3′	Genepharma	N/A
Tgfb1-Mus-1489 antisense sequence 5′-UAUUCCGUCUCCUUGGUUCUU-3′	Genepharma	N/A
Recombinant DNA		
CXCL3 overexpression plasmid	Fenghui Biotechnology	N/A
Software and algorithms		
ImageJ	National Institutes of Health	https://imagej.nih.gov/ij/
GraphPad Prism 8.0 for Mac	GraphPad Prism Software, Inc	https://www.graphpad.com/

RESOURCE AVAILABILITY

Lead contact

Further information and requests for resources and reagents should be directed to and will be fulfilled by the lead contact, Yuan Gao (yuan_gao@fudan.edu.cn).

Materials availability

The plasmids used in this study are available from the lead contact. This study did not generate new unique reagents.

Data and code availability

- Proteomics data have been deposited at Mendeley Data repository and are publicly available as of the date of publication. This paper analyzes existing, publicly available data. These accession numbers for the datasets are listed in the key resources table.
- This paper does not report original code.
- Any additional information required to reanalyze the data reported in this work paper is available from the lead contact upon request.

EXPERIMENTAL MODEL AND STUDY PARTICIPANT DETAILS

Ethics statement

The collection and subsequent analysis of all human samples were conducted in strict compliance with the Declaration of Helsinki, and ethical approval was obtained from the committee of the Huashan Hospital, Fudan University (2011-009). All animal care and experimental procedures were approved by the laboratory animal ethics committee of Fudan University (2022-03-LY-GY-48).

Collection of patient tumor tissues

RCC tumor samples and matching tumor-adjacent tissues were collected from patients undergoing surgical resection in Huashan Hospital of Fudan University. Informed consent was obtained from all subjects (detailed information was shown in Table S2). The collection and subsequent analysis of all samples were conducted in strict compliance with the Declaration of Helsinki, and ethical approval was obtained from the committee of the Huashan Hospital, Fudan University.

Isolation of Cancer-associated fibroblasts

Tissues from patients or Renca cells tumor-bearing Balb/C mice were minced into small pieces and then further digested by collagenase A in DMEM culture medium containing 10% fetal bovine serum (FBS) at 37°C for 2 h. The digested tissue fragments were subsequently seeded in plates and grown in DMEM culture media contained 10% FBS for 2–3 days at 37°C with 5% CO_2 to isolate primary CAFs. The majority of adhering cells were fibroblasts after suspended cells and tissue fragments were removed. The cells were further cultured for 3-5 days to acquire purer fibroblasts. The primary fibroblasts were used from the fourth to the eighth passage and identified by immunofluorescence staining, real-time PCR and western blot analysis. CAFs conditioned medium was collected and filtered to remove cell debris for later use.

Isolation of MEF

MEF was isolated from E13.5 embryos. Briefly, embryos were isolated and the heads, tails, limbs, and most of the internal organs were removed. Then the embryos were minced and digested for10 min by trypsin. Cells were collected and and cultured at 37°C with 5% CO_2 to isolate pure primary MEF.

Cell culture

The 786-O, ACHN, NIH-3T3, MEF and CAFs were cultured with DMEM culture medium containing 10% FBS and 1% penicillin-streptomycin solution. Renca renal cancer cells were cultured with 1640/RMPI culture medium containing 10% FBS, 1% penicillin-streptomycin solution, 0.1 mM NEAA, 1 mM sodium pyruvate and 2 mM L-glutamine (obtained from Procell). All cell lines have been authenticated using short tandem repeat profiling within the last three years. All experiments were performed with mycoplasma-free cells.

Animal experiments

Healthy female Balb/C mice aged 6 to 8 weeks were obtained from Shanghai Lingchang Biotechnology Co., Ltd. (Shanghai, China). All mice were housed in appropriate environment with specific pathogen-free conditions. They were subjected to a 12-h light/dark cycle, living at a temperature of $25 \pm 2°C$ and a relative humidity of 50%, with free access to food and water. For establishment of a subcutaneous Renca tumor model, 1×10^6 Renca cells were resuspended in 100 μL of PBS and subcutaneously injected into the mice. For the CAFs co-transplantation group, 1×10^6 Renca cells and 1×10^6 CAFs were co-injected subcutaneously. When the tumor volume reached approximately 100 mm^3, the mice in each group were treated with PBS or sunitinib or SB225002. As for the lung metastasis model, 1×10^6 Renca cells or combined with same number CAFs were injected by tail vein injection. Drug treatment from the day of model construction. The Control group or Co-CAFs group received 200 μL PBS, and the Sunitinib group received 40 mg/kg of sunitinib orally each day, while SB225002 group received 10 mg/kg of SB225002 intraperitoneally each day. The tumor volume was measured every 3 days. All animal care and experimental procedures were approved by the Biomedical Ethics Committee of Fudan University.

METHOD DETAILS

Cell proliferation and cytotoxicity assay

The cell proliferation was assessed using the CCK-8 kit according to the manufacturer's instructions. Briefly, 786-O, ACHN and Renca cells were seeded in 96-well plates and cultured with CAFs conditioned medium diluted 1:1 with fresh medium (CAFs-CM) or normal fibroblast conditioned medium diluted 1:1 with fresh medium (NFs-CM) for 24 h to evaluate the effect of CAFs on cell proliferation. For sunitinib cytotoxicity, tumor 786-O, ACHN and Renca cells were exposed to sunitinib at various concentrations for a 24 h period with or without CAFs-CM or SB225002. CCK8 solution was then added into the 96-well plates, followed by incubation at 37°C for 1 h. Absorbance was measured at a wavelength of 450 nm, and cell proliferation was compared after conversion into the cell survival rate.

Invasion and migration assays

For the migration assay, 100 μL of tumor cell suspension containing 7.5×10^4 cells were seeded in the upper chamber of each Transwell inserts (8 μm PET membrane, Corning, NY, USA), and 800 μL of culture medium, CAFs-CM (diluted 1:1 with fresh culture medium), culture medium

containing recombinant CXCL3 or SB225002 was added to the lower chamber. The cells were cultured in a humidified incubator at 37°C with 5% CO_2 for 24-36h and stained by crystal violet. For invasion assay, 100 μL of diluted Matrigel matrix was carefully added to the Transwell inserts to form a gel. The subsequent steps were the same as those in the migration assay. The invaded and migrated cells were observed and counted under a microscope.

Wound healing

Horizontal lines were drawn on the back of 6-well plates, and 1×10^5 RCC cells were seeded in plates. Cells were cultured overnight, and a wound was scratched perpendicular to the lines utilizing a pipette tip when the fusion rate reached 100%. Next, the cells were cultured with fresh medium or CAFs-CM at 37°C for 24 h or 36 h, and the images were captured at 0, 24 h, or 36 h after the wound was created. The wound closure rate was then analyzed.

Colony formation

RCC cells were seeded (500 cells/well) in 12-well plates and then cultured with fresh medium or CAFs-CM at 37°C for 7–14 days. Cells were fixed with 4% paraformaldehyde for 10 min, followed by further 10 min of 0.1% crystal violet staining. The number of clones with over 50 cells was counted.

Plasmid or small interfering RNA transfection

The silencing of CXCL3 and TGF-β sequences and its negative control were provided by Shanghai Genepharma Co. Ltd. (Shanghai, China). The siCXCL3 sequences were listed in the key resources table. The CXCL3 (NM_203320) overexpression plasmid (pCDNA3.1-EGFP-PURO) was constructed by Fenghui Biotechnolog Co. Ltd. (Human, China), 5' CMV-F: CTAGAGAACCCACTGCTTAC, 3'BGH-R: TAGAAGGC ACAGTCGAGG. Plasmid or siRNA transfected by Lipofectamine 3000, according to the manufacturer's instructions. The silencing or over-expression efficiency was evaluated by qPCR analysis or ELISA assay.

Real-time PCR analysis

Total RNA was extracted from cells using RNA Isolater Total RNA Extraction Reagent and cDNA was synthesized using the HiScript III All-in-one RT SuperMix. Taq Pro Universal SYBR qPCR Master Mix was employed to measure mRNA expression levels in accordance with the recommendations of the manufacturer. The above three reagents were purchased from Vazyme Biotech Co., Ltd. (Nanjing, China). The real-time PCR primer sequences were listed in Table S1. And β-actin was used as an internal control for data normalization.

Western blot analysis

Protein was harvested from cells with RIPA lysis buffer, and protein concentrations were determined using a bicinchoninic acid kit. For western blot detection, 10 μg of protein was added into each well and separated by a 4–15% BeyoGel Plus Precast PAGE Gel (Beyotime Biotechnology Co., Ltd., Shanghai, China). And proteins were then electro-transferred to polyvinylidene difluoride membranes. Then, the blots were incubated with primary antibody (1:1000) or mouse anti-GAPDH antibody (1:2000) at 4°C overnight. After incubation with horseradish peroxidase-conjugated secondary antibodies (1:2000) for 1 h, protein blots were visualized with an enhanced ECL chemiluminescence detection kit. GAPDH was used as an internal control. All bands were quantified by ImageJ software.

Label-free proteomics sequencing

CAFs were cultured *in vitro* to the fourth to eighth generation, and then, the culture medium was replaced with serum-free culture medium. The cell conditioned medium was collected after 24 h serum-free culture. And conditioned medium from NFs were used as a negative control. Label-free proteomics sequencing was performed to screen for target proteins. Subsequently, the results were analyzed by significance difference analysis and cluster analysis.

Flow cytometry

Renca cells were digested into single-cell suspension after being stimulated by CAFs-CM or CXCL3 for 24 h. Then, cells were stained with FITC anti-mouse CD182 (CXCR2) antibody in the dark for 20 min, and detected on CytoFlex S flow cytometer (Beckman, USA) in accordance with the manufacturer's instructions. The data were analyzed using Flow Jo software.

The Cancer Genome Atlas data analysis

RNA-seq data of 536 RCC samples and 72 normal samples were downloaded from the TCGA database and processed with the R software. The estimate score, stromal and immune scores, CAFs infiltration score, and CAFs proportion were analyzed using ESTIMATE[40] and EIPC (gfellerlab.shinyapps.io/EPIC_1-1/). The seven CAFs score signature reported by Liu et al.[21] were utilized for Kaplan–Meier survival analysis. GSEA (GESA) was used to explore the relationship between enrichment of CXCL3 and activation of ERK and TGF-β signaling pathway in clinical RCC tissues.

QUANTIFICATION AND STATISTICAL ANALYSIS

The data are displayed as Mean $\pm$ SD in bioinformatics analysis or the mean $\pm$ SEM in other experimental data. $*p < 0.05$, $**p < 0.01$, and $***p < 0.001$ were used to determine the statistical significance of differences ($n \geq 3$). Differences among the groups were analyzed using Student's t test or one-way ANOVA for multiple comparisons with Tukey's test. All statistical analysis were performed using GraphPad Prism for Mac (Version 8.4.3, La Jolla, CA, USA).